Advanced Materials Research Vols. 41-42 (2008) pp 69-74
Online available since 2008/Apr/08 at www.scientific.net

doi:10.4028/www.scientific.net/AMR.41-42.69

Contact Pressure of Porous Al_2O_3 Probed by Nanoindentations

Zhong LING[1, a], Shengwang HAO[1,2,3,b]

[1]State Key Laboratory of Nonlinear Mechanics (LNM), Institute of Mechanics
Chinese Academy of Sciences, Beijing 100080, PR China

[2]Department of Applied Physics, Beihang University, Beijing 100083, PR China

[3]School of Civil Engineering and Mechanics, Yanshan University, Qinhuangdao 066004, PR China

[a]lingz@lnm.imech.ac.cn, [b]hsw@lnm.imech.ac.cn

Keywords: porous Al_2O_3; contact pressure; microscale; nanoindentation

Abstract. Contact pressure of porous Al_2O_3 probed by nanoindentation was investigated by dimensional analysis with special attention paid to scaling effects in the mechanical behavior. It was found that, for sample containing small grains and interconnected pores, the contact pressure is manifest dominated by bonding strength of the porous alumina. Whereas the samples with coarse grain and various porous structures exhibit higher contact pressures and smaller residual deformations, which can be attributed to the mechanical response of the solid-phase under current limited peak loads.

Introduction

The mechanical reliability of porous Al_2O_3 depends on pore geometry, grain arrangement in the solid phase and bonding strength [1-5]. In effect, the grain bounding strength dominates the mechanical properties of the porous ceramics. Although several efforts have been made for bonding strength and microstructure effect [4-5], the work related to microstructure effects needs to be verified with tests at nano- microscale.

As one state-of-the-art in situ characterization method, instrumental nanoindentation can be used to probe the mechanical response of systems that are inaccessible via other methods [6, 7]. Recently it has been frequently employed to probe a microscale entity in porous materials and the studies focused load-depth (P-h) behavior which is sensitive to grains or pores beneath indentation [1, 8-12]. In particular, magnitude of contact pressures probed by nanoindentation in porous alumina, containing fine or coarse grains [10], was totally different and relied on alumina grain size. Whether the contact pressure however relates to bonding strength in the porous alumina remains unclear. To understand it well, in current study, dimensional analysis was applied to investigate the contact pressure in the porous alumina.

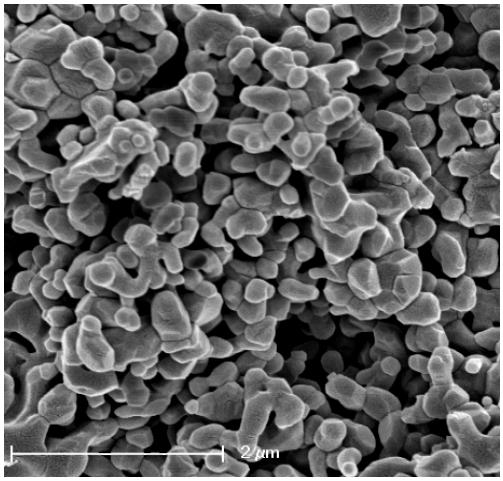

Fig.1 a typical pore structure of sample I (Al_2O_3-grain size: 100-300nm)

Indentation into porous ceramics

Experimental results [10] Porous Al_2O_3 with three grain sizes were tested. Sample I was made from nano-grains of α-Al_2O_3 with a starting size of 50nm sintered in air at 1550℃ for 2 hours. Sample II was fabricated with fine pure α-Al_2O_3 (TM-DAR, particle size range 0.1-0.3μm, surface area 13.6m^2g^{-1}, Taimei Chemical Co. Nagano, Japan), and sintered in air at 1250℃ for 10 minutes. Sample III was made with

alumina powders (AKP50, particle size range 0.1-0.3 μm, surface area 9-16 $m^2 \cdot g^{-1}$, Sumitomo Chemical Co., Osaka, Japan) and sintered as for sample II. Fig.1 shows a typical pore structure of sample I and the porous structure comprises of assembled grains, with interconnected voids. Nanoindentation tests were performed at room temperature with a fully calibrated [6] nanoindenter (CSEM Instrument) equipped with a Berkovich tip (3-face pyramid). Usually the indenter tip is blunt due to wearing and the tip's radius should be taken into account. Fig. 2 shows a schematic of a blunted tip, where a_i is tip's radius and the subscript "i" indicates indenter. The peak load levels on the indenter were preset at 5, 10, 30, 50, 70 and 90mN and the loading rate over the peak load was 2/min ([ΔP/P]/min). The samples were finely diamond- polished till a scratch-free surface was obtained. In each test, the indenter was driven at the above-indicated rate into the specimen till the load reached the preset peak load level and then unloaded gradually to zero. For each peak load, five tests were conducted at different locations in a sample. The resultant indentations were observed by Atom Force Microscopy (AFM) [10]. Table 1 shows main material

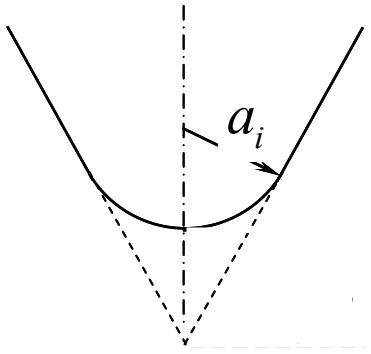

Fig.2 Schematic of a blunted tip

Table 1 main material data and mechanical data (P=10,90mN) of the tested samples*

Sample	Porosity	grain size (nm)	h_m(nm)		ε_{re}(%)		p_f(GPa)	
			h_{10}	h_{90}	ε_{10}	ε_{90}	p_{10}	p_{90}
I (α-Al_2O_3)	0.193	100-300	460	1300	80	80	3.1	3.4
II(TM-DAR)	0.19	200-500	187	540	57	60	20.7	24.4
III(AKP50)	0.16	200-900	147	449	46	53	25.6	37.1

* h_m ε_{re} and p_f are the maximum depth at a peak load, the residual deformation after unloading and contact pressure over an indent, respectively

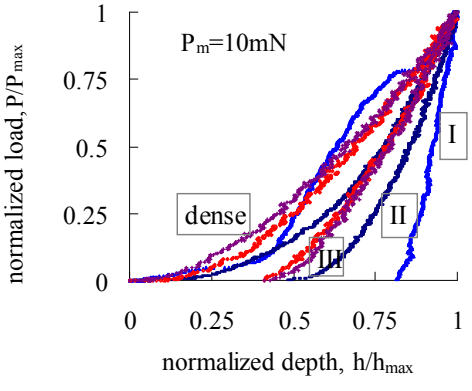

Fig.3 Normalized load-depth for three samples, P_m = 10mN

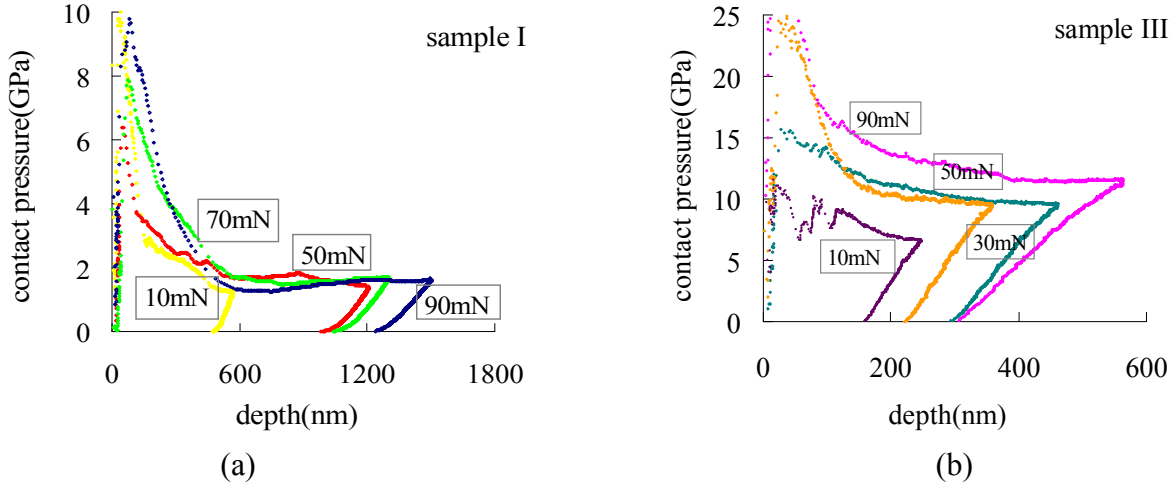

Fig.4 Contact pressure tracks with indenter depth under different peak loads (P_m = 10-90mN), (a) sample I; (b) sample III

and test data for the samples.

Contact pressure, p_f, is defined as mean pressure over project area of an indentation [1], $p_f = P(h_c)/A(h_c)$, where P is peak load and h_c contact depth; $A(h_c)$ is the projected area of the indentation. The residual deformation is $\varepsilon_{re} = h_f / h_m$, where h_f is final residual depth and h_m the maximum depth at the peak load.

Fig. 3 displays the normalized load, P/P_{max}, against the normalized depth, h/h_{max}, of all tested samples under 10mN of peak load. Few pop-in could be seen in the loading parts for sample II and III. The residual deformation ε_{re} obtained in the three samples are followed in the order: $\varepsilon_{reI} > \varepsilon_{reII} > \varepsilon_{reIII}$.

Fig. 4 exhibits the *contact pressure,* in sample I and III, tracking with indentation depth under each peak load, 10-90mN. In sample I, a precipitately decay in contact pressure appears while indentaion depth less than 300nm and then gets to plateau after depths larger than 500nm (Fig.4a). Whereas in sample III, a decay in resultant contact pressures occurrs as indentation depth less than 200nm and then drops gradually till indentation depth getting to the maximum, depending on peak loads (Fig.4b). In this case, a plateau of contact pressure can be seen only under higher peak loads in the sample. The *contact pressures* got in the test are 3-7GPa probed within the depth of 300-1600nm in sample I, 10-25GPa at 200-550nm in sample II and, 20-38GPa at 150-450nm in sample III.

Dimensional analysis - About contact pressure and bonding strength Let A_{0c} as project area of an indentation at contact depth, h_c, for a porous material, A_s is the bonding area [2-4] within A_{0c}. Relative density of the porous material is defined as:

$\rho_p/\rho_s = 1 - f_p = A_s/A_{0c}$ (1)

Where ρ_s, ρ_p are the density of the solid and its porous material, respectively. f_p is porosity and relates to ratio of bounding area and project area, A_s/A_{0c}.

Bonding strength, σ_c, on an indentation is related to total bonding area within the contact area [2,4]:

$$\sigma_c = \frac{P}{A_s} = \frac{P}{A_{0c}}\frac{A_{0c}}{A_s} = p_f\left(\frac{1}{1-f_p}\right), \quad p_f = \frac{P}{A_{0c}} \le \sigma_c\left(\frac{\rho_p}{\rho_s}\right) = \sigma_c(1-f_p) \tag{2}$$

Where p_f is contact pressure on a project area of an indentation and its critical value is rely on bonding strength and porosity of the porous material.

-On dimensional analysis [7]

During loading, load on the tip, P, can be written as:

$$P = F_L(E_s, \nu_s, p_f, \sigma_c, \rho_s; \rho_p, d_g, a_i, h, f_p, \theta) \tag{3}.$$

Where E_s and ν_s are Young's modulus and Poisson's ratio of the solid; d_g, characteristic size of grains (cells) in the porous material; a_i radii of a blunt tip of the indenter; h indentation depth during loading; θ is angle of indenter tip .

Let E_s and h as principal variables in Eq.3, one has:

$$\frac{P}{E_s h^2} = F_{L1}\left(\nu_s, \frac{p_f}{E_s}, \frac{\sigma_c}{E_s}; \frac{d_g}{h}, \frac{a_i}{h}, \theta, f_p\right) \tag{4}$$

Where $\frac{P}{E_s h^2}$ and $\frac{h_c}{h}$ would be controlled by p_f, σ_c and d_g as well as a_i. As ν_s, θ and f_p are dimensionless, for a given porous material, Eq.4 is reduced to:

$$\frac{P}{E_s h^2} = F_{L1}\left(\frac{p_f}{\sigma_c}; \frac{d_g}{h}, \frac{a_i}{h}, f_p\right) \tag{4'}$$

Consequently, as $P/E_s h^2$ is independent on depth due to $P \propto h^2$ [7], p_f/E_s varies with σ_c/E_s, d_g/h and a_i/h or, p_f under peak load, P, depends on σ_c, d_g, a_i and h.

Because unloadig takes place after loading during which the indentation reachs the maximum depth, $h=h_m$, and the load is at its peak value, $P=P_m$; and after completely unloading, P=0 and final depth $h=h_f$, the equation for completely unloading is, using dimensional analysis [7],

$$0 = F_{L1}(\nu_s, \frac{p_f}{E_s}, \frac{\sigma_c}{E_s}; \frac{d_g}{h_m}, \frac{h_f}{h_m}, \theta, f_p) \tag{5}$$

Thus, $\frac{p_f}{E_s} = F_{L1}(\nu_s, \frac{d_g}{h_m}, \frac{\sigma_c}{E_s}, \frac{h_f}{h_m}, \theta, f_p)$, where $h_f/h_m=\varepsilon_{re}$ is residual deformation. In this case, p_f/E_s is depending on σ_c, d_g/h_m and ε_{re}.

Unlike indentation into dense materials, Eqs.4-5 figure out that, besides bonding strength, indentation depth and porosity, contact pressure probed by indentation is dependent on d_g, grain size of the porous structure.

Results and discussion In this section discussions are for the resultant experimental data probed in the tested porous alumina.

For the results during loading firstly.

(1) For sample I, its grain size is as same as indenter's radius, $d_g \sim a_i$

(i) $h<d_g \sim a_i$, initial indentation

At initial indentation, $h<a_i$. As $d_g \sim a_i$, from Eq.4', p_f/E_s gets larger while $h \ll a_i \sim d_g$. It shows that contact pressure p_f reached at higher level at inital penetration. As shown in Fig.4a, a decay in contact pressure appears at depth <300nm in sample I, being resulted in grains' crushing while p_f's magnitude is high to its critical value. Similar decay in contact pressure was reported and addressed as indenation size effects in previous studies [1,11,12]. With depth larger, it leads to form pop-in during loading in Fig.3 or undulant steps in decay in Fig.4a.

(ii) $h \geq d_g \sim a_i$, deeper indentation, while tip's depth larger than its radii, a_i,

With indentation depth getting larger and being compared with grains size, $h \sim d_g \sim a_i$, p_f/E_s depends on σ_c/E_s for $a_i/h \to 1$. In this case, crushing occurs while p_f's magnitude reaches its critical value. In particular, p_f/E_s is completely dependent on σ_c/E_s while $h>>d_g \sim a_i$. That is, no matter how higher the peak load is, contact pressures probed by indentation keeps in a constant. As plotted in Fig.4a, in the sample containing 100-300nm grains, contact pressure is unvaried with depth increasing while $h>$ 500nm. The contact pressure is 3.1-3.4GPa and this critical value is consistent with that presented by Latella et al [13].

(2) For sample II and III, the grains' size is larger than indenter's radius, $d_g>a_i$

(i) $h< a_i <d_g$, initial indentation

As $\frac{d_g}{h} > \frac{a_i}{h} \geq 1$, it is the same with the discussion in the case of initial indentation while $d_g \sim a_i$, i.e. p_f/E_s varies with σ_c/E_s and a_i/h. As $h<a_i$, the smaller the dpeth h, the higher the contact pressure p_f is. In general, contact pressure p_f is not easy to exceed its critical value due to $d_g>a_i>h$. Whereas at $a_i=h$, p_f/E_s depends on value of d_g/h. Obviously, analysis to contact pressure decay here looks like to that for the sample with small grains at initial penetration. As shown in Fig.4b, at initial indentation, contact pressure decay can be seen in the smaple III.

(ii) $a_i <h <d_g$, during indentation

In the limited case of $h>>a_i$, as $h<d_g$, p_f/E_s is dominated by σ_c/E_s and d_g/h. One has:

$$\frac{P}{E_s h^2} = F_{L1}(\nu_s, \frac{p_f}{\sigma_c}; \frac{d_g}{h}, \theta, f_p) \tag{6}$$

Obviously, with depth being larger, contact pressure, p_f, would decrease gradually. However in Fig.4b, resultant p_f gets up while peak load increased. As shown in Table 1, grain size is about 200-500nm for sample II and 200-900nm for sample III. Whereas the maximum indentation depth in both sample II and III, under the maximum peak load, 90mN, is less than grain size, i.e. $d_g/h>1$. In this case, contact pressure no longer follows Eq.2, since a larger grain, compared with limited indentation depth, seems to be a solid phase with no pores. As no pore and no crushing, to reach at the critical contact pressure, the higher load is needed. What shown in Fig.4b indicates that, at initial indentation, contact pressure decay is caused by tip's radius and the pleadou is regarded as response solid phase to the indentation. In addition, current case is based on Berkovich indenter with tip's radius, 100-200nm. If the tip's radii larger enough, i.e. $a_i >> d_g$, the discussion is similar to that for the case $h<d_g<a_i$. *However* the case of $a_i >> d_g$, d_g=200~900nm, is beyond current testing range and shall be discussed in further study.

As foregoing, unloading takes place after depth at its maximum value, $h=h_m$, and after completely unloading, P=0 and $h=h_f$, which is not related to tip's radius due to $h_m >> a_i$. Thus p_f/E_s is expressed as

$$\frac{p_f}{E_s} = F_{L1}(v_s, \frac{d_g}{h_m}, \frac{\sigma_c}{E_s}, \frac{h_f}{h_m}, \theta, f_p) \tag{7}$$

p_f depends on σ_c, d_g/h_m and ε_{re}. Two cases will be discussed in followings.

For sample I with fine grains, $d_g/h_m << 1$, p_f/E_s is dominated by σ_c and ε_{re}. Once the value of p_f reaches its critical value given by Eq.2, crushing occurs with ε_{re} keeps increasing, as shown in Table 1.

For sample II and III with coarse grains, their d_g/h_m maybe larger than 1. So p_f/E_s for the both samples would depend on d_g/h_m and ε_{re}. Only while reaching high peak load, scale of h_m can be larger than that of grains, p_f may get at its critical value to cause crshing. However, in current study, peak loads are limited and the case seems to be the same with that in dense phase without pores. Also, as shown in Table 1, in both sample with coarse grains, the higher the peak load, the larger the residual strain, which is consistent with what predicted by Eq.7.

Furthermore, noticing $d_g/h_m >> 1$ in the sample II, III and $d_g/h_m << 1$ in sample I, and assuming the porosity for three samples is almost the same, under the same peak load, contact pressure in each sample meets followings:

$$\frac{p_f}{E_{s\,|II,III}} = F_{L1}(\frac{\sigma_c}{h_m}, \frac{d_g}{h_m}, \frac{h_f}{h_m}, \theta, f_p)_{|II,III} > \frac{p_f}{E_{s\,|I}} = F_{L1}(\frac{\sigma_c}{h_m}, \frac{h_f}{h_m}, \theta, f_p)_{|I} = const.$$

This has also been verified in experimental observations, in which contact pressure of samples II and III is higher than that of sample I (Table1).

Summary

Contact pressure of porous Al_2O_3 probed by nanoindentation was investigated by dimensional analysis. For sample I with small grains, the contact pressure exhibited, during loading, a decay at shallow depth and then a plateau while reaching its critical value. Dimensional analysis deduced that, at initial indentation, the decay in contact presure was caused by higher contact pressure reaching grains' bonding strength. In this case, higher contact pressure was resulted from the small indentation depth compared with tip's radius. During indentation, the constant contact pressure was dominated by bonding strength of the porous ceramcis. For the samples containing coarse grains, higher contact pressures probed at limited depth could be attributed to local responses of the solid-phase under current limited peak loads. Also, as $d_g/h_m >> 1$ in the sample II, III and $d_g/h_m << 1$ in sample I , the experimental result of $p_{f|II,III} > p_{f|I}$ is reasonable.

Acknowledgements

The author, Zhong LING, would like to thank Dr J MA, Nanyang Technological University (NTU), Singapore, for the assistances on supplying the porous alumina samples. Thanks to Prof. QM TAN,

Institute of Mechanics, Chinese Academy of Sciences, for valuable discussions on dimensional analysis. Also Zhong LING would like to express deepest gratitude to TCT Exchange fellowship, Nanyang Technological University (NTU), Singapore, for the opportunity to study porous ceramics and its microstructure effect in Department of MPE, NTU, during the spring of 2003.

References

[1] L. J. Gibson and M. F. Ashby, Cellular Solids: Structure and properties, 2nd edition, Cambridge Press, 1997

[2] J.C.Wang, J. Mater. Sci. Vol. 19(1984)801-814

[3] R. W. Rice, J. Am. Ceram. Soc. Vol.76 (1993), p.1801

[4] Z.Y. Deng, et al, J. Am. Ceram. Soc., Vol.84 (2001) p.238

[5] D. J. Green, et al, J. Am. Ceram. Soc. Vol.78 (1995) p.266

[6] W.C. Oliver and G. M. Pharr, J. of Mater. Res. Vol. 7(1992) p.1564

[7] Y.T. Cheng and C.M. Cheng, Int. J. Solids & Struc., Vol. 36(1999)p.1231

[8] A.G. Alcal, et al, Nanotechnology, Vol.13 (2002) p.451

[9] Y. Toivola, et al, J. Mater. Res. ,Vol. 19 (2004) p.260

[10] Z. Ling et al, Mater. Sci. Engng. A (in press) doi:10.1016/j.msea.2006.10.195

[11] E.M. Andrews et al, Int.J.Mech.Sci., Vol.43(2001) p.715

[12] A.M. Hodge et al, Acta Materialia, Vol. 55 (2007), p. 1343

[13] B.A. Latella et al, J.Am.Ceram. Soc., Vol. 80 (1997), p.1027

Structural Integrity and Failure, 2008
10.4028/www.scientific.net/AMR.41-42

Contact Pressure of Porous Al_2O_3 Probed by Nanoindentations
10.4028/www.scientific.net/AMR.41-42.69

DOI References
[9] Y. Toivola, et al, J. Mater. Res. ,Vol. 19 (2004) p.260
doi:10.1557/jmr.2004.0030
[10] Z. Ling et al, Mater. Sci. Engng. A (in press)
doi:10.1016/j.msea.2006.10.195
[12] A.M. Hodge et al, Acta Materialia, Vol. 55 (2007), p. 1343
doi:10.1016/j.actamat.2006.09.038